Combining commercial microwave links and weather radar for classification of dry snow and rainfall

Erlend Øydvin[1], Renaud Gaban[1, 5], Jafet Andersson[2], Remco (C. Z.) van de Beek[2], Mareile Astrid Wolff[1, 5], Nils-Otto Kitterød[4], Christian Chwala[3], and Vegard Nilsen[1]

[1]Faculty of Science and Technology, Norwegian University of Life Sciences, Ås, Norway
[2]Swedish Meteorological and Hydrological Institute (SMHI), 601 76 Norrköping, Sweden
[3]Institute of Meteorology and Climate Research, Karlsruhe Institute of Technology, Campus Alpin, Garmisch-Partenkirchen, Germany
[4]Faculty of Environmental Sciences and Natural Resource Management, Norwegian University of Life Sciences, Ås, Norway
[5]Norwegian Meteorological Institute, Oslo, Norway

Correspondence: Erlend Øydvin (erlend.oydvin@nmbu.no)

Abstract. Differentiating between snow and rainfall is crucial for hydrological modeling and understanding. Commercial Microwave Links (CMLs) can provide rainfall estimates for liquid precipitation, but show minimal signal attenuation during dry snow events, causing the CML time series during these periods to resemble non-precipitation periods. Weather radars can detect precipitation also for dry snow, yet they struggle to accurately differentiate between precipitation types. This study introduces a new approach to improve rainfall and dry snow classification by combining weather radar precipitation detection with CML signal attenuation. Specifically, events where the radar detects precipitation, but the CML does not, are classified as dry snow. As a reference method, we use weather radar with the precipitation type identified by the dew point temperature at the CML location. Both methods were evaluated using measurements from disdrometers located within 8 km of a CML, taken as ground truth. The analysis used data from Norway, including 550 CMLs in December 2021 and 435 CMLs in June 2022. Our results show that the use of CMLs can improve the classification of dry snow and rainfall, presenting an advantage over the reference method. In addition, our research provides valuable insight into how precipitation at temperatures around zero degrees, such as sleet or wet snow, can affect CMLs, contributing to a better understanding of CML applications in colder climates.

1 Introduction

The precipitation phase is crucial for hydrological processes in cold regions (Loth et al., 1993). Understanding the type of precipitation aids in applications such as adjusting rain gauges for wind undercatch (Kochendorfer et al., 2022) and modeling hydrological responses such as flooding. Moreover, specific precipitation conditions, like freezing rain, can disrupt power lines and impede traffic, and snow may cause transportation blockages. Rain-on-snow events have also been associated with significant flooding (McCabe et al., 2007), and with slush avalanches (Hestnes, 1985).

The formation of precipitation is a complex process. In the high and mid-latitudes, most precipitation originates from mixed-phase or cold clouds, that is clouds containing ice (Stewart et al., 2015). The ice crystals grow in size and mass through different

micro-physical mechanisms such as vapor deposition and riming, until they reach a sufficient mass to sediment out of the cloud base (Stewart, 1992). A necessary condition for a cloud to generate solid phase-precipitation is that its temperature is negative. Unless the temperature of the layer of atmosphere underneath the cloud remains below zero degrees, the precipitating ice

25   will start melting before reaching the ground (Lamb and Verlinde, 2011). The melting process is not instantaneous and an ice particle can fall hundreds of meters before melting completely. Therefore, originally solid precipitation can reach the ground in any intermediate state between solid and liquid, depending on the elevation of the zero-degree isotherm (Paulson and Al-Mreri, 2011; Harpold et al., 2017). The melting process is also influenced by other elements of the atmospheric conditions. Specifically, the stability of the atmosphere and the atmospheric humidity profile have a significant influence because the liquid

30   water formed from melting of ice will tend to evaporate in dry conditions, cooling the atmosphere in turn and hampering further melting (Harder and Pomeroy, 2013). Atmospheric conditions that determine the precipitation phase can change relatively quickly. For instance, a study by Marks et al. (2013) observed a significant increase of the elevation of the melting layer within the same precipitation event. Determining the precipitation phase at the ground level is therefore difficult and models predicting the precipitation phase typically need to be calibrated and validated against measurements (Harpold et al., 2017).

35   There are several ways of determining the precipitation phase using ground based observations. For example, Marks et al. (2013) used a combination of a tipping bucket rain gauge and a heated weighing gauge. During rain, the devices record similar amounts, but when it snows, the snow clogs the funnel of the tipping bucket, leaving only the weighing gauge to record precipitation. Other studies, such as Matsuo et al. (1981), used human observers to directly observe precipitation phase. More advanced methods include using weather radars, especially with dual polarization, to estimate and classify precipitation

40   phase (Grazioli et al., 2015; Chandrasekar et al., 2013). Disdrometers also estimate precipitation phase based on the physical properties of hydrometeors (size and fall velocity), with semi-empirical knowledge of how these properties vary with type (Löffler-Mang and Joss, 2000; Yuter et al., 2006). However, each method has its own limitations. Rain gauges, providing point measurements, have limited spatial representation and can be affected by wind-induced errors (Førland et al., 1996; Nešpor and Sevruk, 1999; Kochendorfer et al., 2022; Wolff et al., 2015). Human observations can be subjective and are not suitable for

45   continuous high-rate monitoring. Weather radars can suffer from beam blockage (Berne and Krajewski, 2013), overshooting, and still have difficulties linking the estimated precipitation type to ground measurements (Harpold et al., 2017; Elmore, 2011). Like rain gauges, disdrometers are limited in spatial representation and can experience errors such as splashing of drops against nearby structures, drops falling on the edge of the measuring area, and wind altering the drop trajectories (Friedrich et al., 2013).

      Precipitation phase estimation often employs a temperature model. This involves modeling the rain-snow transition based

50   on temperature using for instance a single temperature threshold to separate rain and snow, or two thresholds that define mixed precipitation in between the two thresholds (Kienzle, 2008). Jennings et al. (2018) found that, when using a single temperature threshold, the threshold separating rain from snow varies geographically, ranging from -0.4 to 2.4 for most stations and with colder thresholds near the coast and warmer thresholds in mountains. They also found that models incorporating humidity performed better than models considering air temperature alone, which is confirmed by other studies (Matsuo et al., 1981).

55   Although some studies do not observe any benefit of including humidity (Leroux et al., 2023), humidity is thought to be an important parameter since the atmospheric moisture level affects the melting and evaporating precipitation, influencing whether

precipitation reaches the ground as solid or liquid (Kuhn, 1987). One common measure combining humidity and temperature is the dew point temperature, which is the temperature at which the air would become saturated with water vapor at constant pressure and moisture content (Lawrence, 2005). In a dry atmosphere, the dew point temperature is significantly lower than the air temperature. In these conditions, melting is not favored and snow can be observed at positive air temperatures. Conversely, the dew point and the air temperatures are equal if the air is saturated, and solid precipitation will more likely have melted before reaching the ground if the air temperature is above 0 degrees (Feiccabrino, 2020; Harder and Pomeroy, 2013, 2014). However, a large degree of uncertainty in precipitation type classification remains even when temperature and humidity are combined. Harpold et al. (2017) suggest that current phase transition models are too simple to capture the process, especially in complex terrain. They suggest, for instance, to improve this by better use of other atmospheric information and enhancing the validation network with ground measurements such as disdrometers.

Commercial microwave links (CMLs) are radio links between radio communication towers. In the mid-2000s, it was demonstrated by Messer et al. (2006) and Leijnse et al. (2007) that CMLs can be used to estimate rainfall. This is due to the relationship between signal attenuation and rainfall intensity. At around 30 GHz, the relation is close to linear, making it easier to estimate the average rainfall intensity along the CML path. Among other applications, CMLs have been used to estimate countrywide rainfall (Graf et al., 2020; Overeem et al., 2016), transboundary rainfall fields (Blettner et al., 2023) and CMLs have proven useful for estimating runoff in urban hydrology (Pastorek et al., 2023). A crucial step in CML rainfall estimation is the detection of rainfall, often called wet periods, in the CML time series. There are several ways of doing this, for instance by classifying a period as wet when the standard deviation of a moving window is larger than a predefined threshold (Schleiss et al., 2013; Graf et al., 2020), by using pre-trained classification models (Polz et al., 2020; Øydvin et al., 2024) or by including information from nearby CMLs (Overeem et al., 2011). It is also possible to use weather radar to estimate the CML wet period as done in Overeem et al. (2016).

Classification of precipitation types other than rain using CMLs has previously been investigated by Cherkassky et al. (2014). The authors used the fact that snow, sleet (defined as a mixture of snow and rain), and rainfall are affected differently by different CML frequencies. Thus, by using three CMLs operating at different frequencies in the same area, they were able to distinguish periods of sleet and rainfall, albeit only for two precipitation events, each lasting three days. Ostrometzky et al. (2015) expanded on this study by using four CMLs operating at different frequencies and clustered at a single path to estimate the precipitation amounts generated by rainfall and sleet. The study investigated four precipitation events lasting a total of 16 days. A limitation of both of these studies is that they focus on a low number of CMLs over a few days. It is not known how well these methods generalize to longer time series and larger CML networks. Other studies have focused on how CMLs are affected by colder climates. Hansryd et al. (2010) reported that heavy snowfall caused minimal signal attenuation, while a mix of rain and snow, caused higher signal attenuation. van Leth et al. (2018) observed that during an event with a mixed precipitation the CMLs experience a strong signal attenuation which persisted for about 10 minutes after the precipitation event, possibly due to melting of snow off from the antenna cover. Graf et al. (2020) and Overeem et al. (2016) reported that CMLs tend to overestimate the precipitation amount during winter months. Both attributed this overestimation to melting snow, which is known to cause up to four times the attenuation compared to rainfall, depending on the mixture of snow and rain (Paulson and

Al-Mreri, 2011). Dry snow, on the other hand, is known to cause signal attenuation so low that it cannot be detected by CMLs (Pu et al., 2020; Paulson and Al-Mreri, 2011; Hansryd et al., 2010).

In this study, we explore the viability of classifying dry snow by exploiting the fact that dry snow causes unnoticeable
95 attenuation in the CML data. This is done by first using the weather radar to detect precipitation and then classifying the precipitation type based on whether the CML detects rainfall or not. We compare these estimates to ground truth observations from disdrometers operated by the road authorities in Norway, as well as a reference method that uses weather radar and dew point temperature to estimate the precipitation phase.

2 Methods

2.1 CML data
100

The CML dataset was provided by Ericsson and consists of 2777 CMLs spread out across Norway. Each CML records the transmitted and received signal strength every minute for data from two months: December 2021 and June 2022. The CML signal attenuation, often called total loss (TL), was computed by subtracting the received signal strength from the transmitted signal strength. In our dataset, there were some outliers where the transmitted signal strength was less than -50 dBm. These
105 signals produced negative TL values, likely due to recording errors. We opted to completely remove CMLs with transmitted signal strength less than -50 dBm such that the remaining CMLs did not have any negative TL values. We also removed CMLs with more than 15% missing values. This resulted in 2179 CMLs for the summer dataset and 2345 CMLs for the winter dataset. Next, as suggested by Graf et al. (2020), we removed erratic CMLs where the 5 hours moving window standard deviation exceeded the threshold of 2 dBm more than 10 % of the month and noisy CMLs where the 1-hour moving window standard
110 deviation exceeded the threshold of 0.8 dBm more than 33 % of the month. Then CML derived rain rates were estimated using the *pycomlink* software (Chwala et al., 2023) and a similar workflow as described in Graf et al. (2020), Blettner et al. (2023) and Polz et al. (2020). For the classification of rainy periods, we used the convolutional neural network (CNN) developed by Polz et al. (2020), as this model was trained on hourly data and this study also evaluates estimates at an hourly resolution. The baseline was estimated by using the average signal attenuation 5 minutes before a rainy period. Water droplets forming on
115 the antenna cover cause additional attenuation, which we accounted for by using the semi-empirical wet antenna attenuation model proposed by Leijnse et al. (2008), with the refined parameters suggested by Graf et al. (2020). Finally, the rainfall rate was computed using the k-R relation, with parameters defined by ITU (2005).

2.2 Radar data

Weather radar data for Norway was downloaded from THREDDS (2024), a data hosting platform for gridded meteorological
120 data run by the Norwegian Meteorological Institute. The radar product is developed from 12 weather radars in Norway. These radars are combined using a Constant Altitude Plan Position Indicator (CAPPI). The final result is a grid with a spatial resolution of 1 km by 1 km and a temporal resolution of 5 minutes. Seaclutter and other large peaks in the data are removed, and

groundclutter is identified and corrected using surrounding data. The radar reflectivity (Z [dBz]) is converted to precipitation rates (R [mm/h]) using the Marshall-Palmer relation (Marshall and Palmer, 1948). Radar precipitation rates were estimated along all CMLs using the weighted grid approach provided by *pycomlink*. Then, in line with Polz et al. (2020), time steps with weather radar rainfall rates above 0.1 mm/h were considered rainy.

2.3 Disdrometer data and co-located CMLs

As ground truth for the precipitation type, we used disdrometer data from the Norwegian road authorities. They use two types of disdrometers, namely the OTT Parsivel and OTT Parsivel[2]. The disdrometer data was downloaded from Frost (2024), a data hosting platform for meteorological observations run by the Norwegian Meteorological Institute. This dataset also contains precipitation type observations from other sensor types, such as the Vaisala PWD12/31 and DRD11A. Using a registry provided by the road authorities, we selected time series which was generated using the OTT Parsivel and OTT Parsivel[2]. This was done to ensure a more controlled comparison between sensors. The disdrometers are placed at least 4 meters above the road at automated meteorological stations located along the roads in Norway and provide an estimate of the precipitation type every 10 minutes. The instruments classify precipitation as light rain, rain, snow, and hail. No precipitation, or dry weather, is denoted *dry* in the following. We simplified the classification by merging the classes light rain and rain since they should appear similar in the CML and radar. Additionally, since hail events were rare in the dataset (less than 0.01%) and were not of interest to our study, we set time steps where the disdrometer recorded hail to dry. This adjustment resulted in a negligible error while simplifying the methodology. Thus from the simplifications, the disdrometers only report 3 classes: dry, rain and snow. Pairs of CMLs and disdrometers within 8 km of each other were identified using methods from poligrain (2024) and CMLs longer than 8 km were removed. The threshold of 8 km was a trade-off between getting a large number of CML-disdrometer pairs, while still maintaining good correlation between the pairs. This resulted in 376 CMLs and 83 co-located disdrometers for December 2021 and 304 CMLs and 60 co-located disdrometers for June 2020. We refer to these as the winter and summer datasets respectively. The CMLs used in the study had signal quantization equal to 0.3 dBm, lengths ranging from 0.4 to 8 km and operated at frequencies between 10 to 40 GHz, with the majority (90 percent) operating above 18 GHz (Fig. 1).

2.3.1 Temperature, humidity and dew point temperature

Temperature and humidity data were downloaded from THREDDS (2024). The data is a downscaled version of ERA5 data on a 1 km grid with a temporal resolution of 1 hour (MET, 2024; Lussana et al., 2021, 2019). It should be noted that model data carries inherent uncertainties due to factors like model assumptions and the data down-scaling, and thus the model data used do not perfectly represent the ground truth. For each CML, we extracted the temperature and humidity at the midpoint of the CML. To account for air humidity we calculated the dew point temperature using the approximated relation with air temperature provided by Lawrence (2005), given as

$$T_d = T_a - ((100 - RH)/5), \tag{1}$$

where T_d (°C) is the dew point temperature, T_a (°C) is the air temperature and RH (%) is the relative humidity.
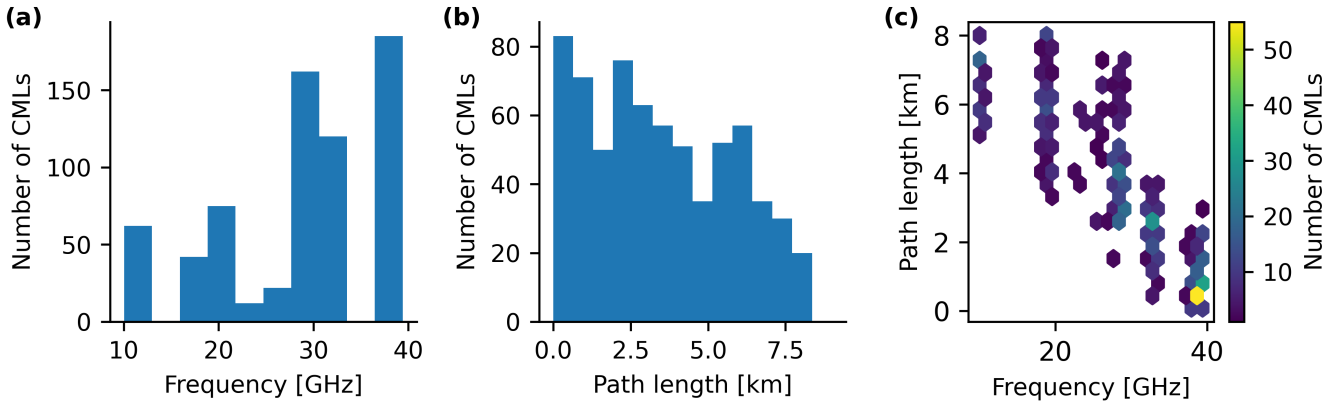
Figure 1. CML characteristics for the summer and winter dataset. **(a)** Distribution of CML frequencies. **(b)** Distribution of path lengths. **(c)** Relationship between path length, frequency, and number of CMLs.

2.4 Classification of rainy and snowy hours using the disdrometers, the CML-radar (CR) method and the radar-temperature (RT) method

The weather radar (5-minute resolution), temperature model (60-minute resolution), CML (1-minute resolution), and disdrometer (10-minute resolution) provide estimates at different locations and with varying time resolutions. This lack of synchronization could potentially lead to erroneous comparisons. To address this issue, we aggregated the precipitation type estimates to hourly intervals to help smooth out these differences.

The "CML-radar" (CR) method uses CML wet periods, as predicted by the wet-dry estimation method, to classify precipitation as rain. Next, since the CMLs are not noticeably attenuated by dry snow, radar precipitation without corresponding CML precipitation is classified as snow. To aggregate the CR estimates to hourly resolution, we classified hours as rainy if the CML rainfall classification algorithm recorded any rainfall, snowy if the radar estimated any precipitation but the CML did not estimate rainfall, and dry otherwise. The "radar-temperature" (RT) method uses surface temperature and weather radar to determine precipitation occurrence and precipitation type. As recommended by Harder and Pomeroy (2014), humidity is accounted for by using the dew point temperature. The RT method then works by estimating the average precipitation along the CML, and classifying precipitation above a dew point temperature threshold as rain and below the threshold as snow. The dew point temperature was evaluated at the pixel closest to the center of the CML and was, in line with Marks et al. (2013), set to 0 °C. Combining humidity-corrected temperature models with weather radar is a common method and is often used as a reference method (Casellas et al., 2021; Saltikoff et al., 2015; Gjertsen and Ødegaard, 2005). To aggregate the RT estimates to hourly resolution we classified hours as dry if the radar observed no precipitation. If the radar observed precipitation, we classified the hours as rainy or snowy based on whether the dew point temperature was above or below 0 degrees, respectively. For the disdrometers, we classified hours as rainy if the disdrometer recorded any rain during that hour, snowy if the disdrometer recorded snow but no rain, and dry otherwise.

Table 1. Confusion matrix for binary classification. The positive class typically represents snow, rain, or both, while the negative class represents all other conditions not included in the positive class.

	Predicted: Negative	Predicted: Positive
Ground truth: Negative	True Negative (TN)	False Positive (FP)
Ground truth: Positive	False Negative (FN)	True Positive (TP)

The drawback of the aggregation method is that we overestimate the number of rainfall events, introducing more uncertainties in the results. However, we consider this an acceptable trade-off as it allows for a more consistent analysis. The effects of the aggregation method are evaluated further in the discussion.

2.5 Metrics

In this study we will consider both binary classification (for instance, rain and not-rain) and multiclass classification (rain, snow and dry). A common tool for visualizing the performance of a classification algorithm is to use a confusion matrix. It compares the ground truth labels with the predicted labels, allowing us to understand the types of errors made by the classifier. In this study the classifier is either the CR or RT method and the ground truth is the disdrometers. In the binary case, the labels are categorized as either negative or positive (Table 1). Using this confusion matrix, several metrics can be defined. We will first consider the the accuracy score, which relates the proportion of true results by the total number of cases examined such that

$$\text{Accuracy} = \frac{\text{TN} + \text{TP}}{\text{TN} + \text{TP} + \text{FP} + \text{FN}}. \tag{2}$$

Because of its simplicity, accuracy is a widely used metric, but it may not always be the best indicator of classifiers performance, especially in cases of imbalanced datasets. To better understand the performance of the classifiers it is therefore common to consider other metrics as well. The precision score focuses on the classifiers positive predictions and provides the ratio between the false and true positive predictions, such that

$$\text{Precision} = \frac{\text{TP}}{\text{TP} + \text{FP}}. \tag{3}$$

It is also common to consider the recall score, which gives the proportion of reference positive cases predicted by the classifier

$$\text{Recall} = \frac{\text{TP}}{\text{TP} + \text{FN}}. \tag{4}$$

Since any classifier typically must strike a balance between false positives and false negatives, improving the precision comes at the expense of the recall. To consider both recall and precision, the F1 score estimates the harmonic mean of the precision and recall, combining these two metrics such that

$$\text{F1} = 2 \times \frac{\text{Precision} \times \text{Recall}}{\text{Precision} + \text{Recall}} = \frac{2\text{TP}}{2\text{TP} + \text{FN} + \text{FP}}. \tag{5}$$

We also use the Matthews correlation coefficient (MCC) to quantify the performance of the classification methods. The MCC is a metric that has been shown to outperform the accuracy and F1 score on imbalanced datasets, by indicating a good correlation only when the classifier performs good on both positive and negative cases (Chicco and Jurman, 2020). The MCC is given by

$$MCC = \frac{TP \cdot TN - FP \cdot FN}{\sqrt{(TP + FP) \cdot (TP + FN) \cdot (TN + FP) \cdot (TN + FN)}}. \tag{6}$$

The accuracy, precision, recall and F1 score reach their best value at 1 and worst score at 0. The MCC score of 1 indicates a perfect prediction, 0 indicates a random guess and -1 is a perfect inverse prediction.

In the multiclass case, the hourly predicted estimates compared to the hourly ground truth can be summarized in a multiclass confusion matrix, see Table 2. The accuracy score can be extended to the multiclass case as follows

Table 2. Multiclass confusion matrix of the ground truth (disdrometer) and predictions (CR and RT method).

	Predicted: Dry	**Predicted: Rain**	**Predicted: Snow**
Ground truth: Dry	True Dry	False Rain	False Snow
Ground truth: Rain	False Dry	True Rain	False Snow
Ground truth: Snow	False Dry	False Rain	True Snow

$$Accuracy = \frac{True\ dry + True\ rain + True\ snow}{Total\ number\ of\ instances}. \tag{7}$$

The precision, recall and F1 scores are slightly more complicated to generalize, as they involve selecting specific parts of the binary confusion matrix. In this work we generalized the precision, recall and F1 scores using macro averaging, which works by evaluating each class (dry, rain snow) individually and then averaging them into a single number.

Following Gorodkin (2004), the MCC metric can be generalized to n classes, providing a balanced metric that uses the full confusion matrix (Jurman et al., 2012). The MCC between the reference x and the predictions y for the multiclass case is given by

$$MCC = \frac{\text{cov}(X,Y)}{\sqrt{\text{cov}(X,X) \cdot \text{cov}(Y,Y)}}, \tag{8}$$

where

$$\text{cov}(X,Y) = \frac{1}{N} \sum_{k=1}^{N} \text{cov}(X_k, Y_k), \tag{9}$$

where N is the number of classes and $\text{cov}(X_k, Y_k)$ is the covariance between the reference X_k and the predictions Y_k for class k. All metrics were computed using *scikit-learn* (Pedregosa et al., 2011).
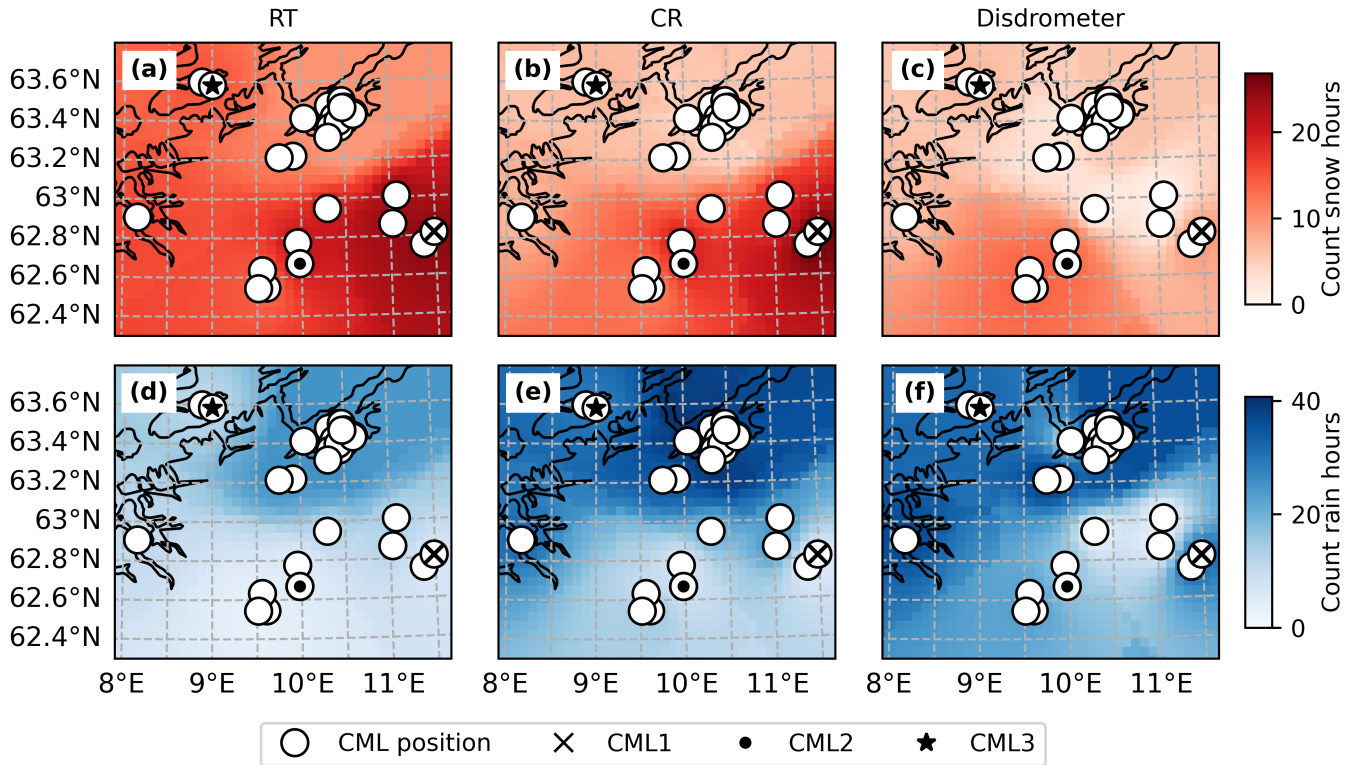
Figure 2. Interpolated count of rainy **(a, b, c)** and snowy **(d, e, f)** hours for the RT method **(a, d)**, CR method **(b, e)** and disdrometers **(c, f)** over a 2-day period starting on the 18th of December 2021. The Trondheim fjord and Norwegian coast (black line) are in the north and west, while the Dovre mountains are in the south. White circles indicate the (distorted) positions of the CMLs. The black x, dot, and star represent the locations of CML1, CML2, and CML3, respectively, with their time series shown in Fig. 3, Fig. 4, and Fig. 5. The maps were interpolated using inverse distance weighting, with the midpoint of the CML indicating its position.

3 Results

3.1 Case study

To illustrate the RT and CR method, we first focus on a case study performed over a large area in mid-Norway, covering 36 CML-disdrometer pairs over a two day period from the 18th to the 20th of December 2021 (Fig. 2). The area spans from the Trondheim fjord and Norwegian coast in the north and west, to the Dovre mountain in the south. For each CML we counted the number of snowy and rainy hours estimated by the RT method **(a, d)**, CR method **(b, e)** and the nearby disdrometer **(c, f)**. The total snowy and rainy hours were then interpolated using inverse distance weighting, with the midpoint of the CML indicating its position. We can observe that at the location of CML1 and CML2 (mountainous areas) the RT and CR method estimates more snow and less rain compared to the disdrometers. At the location of CML3 the RT method estimates more snow and less rain compared to the CR method and disdrometers.
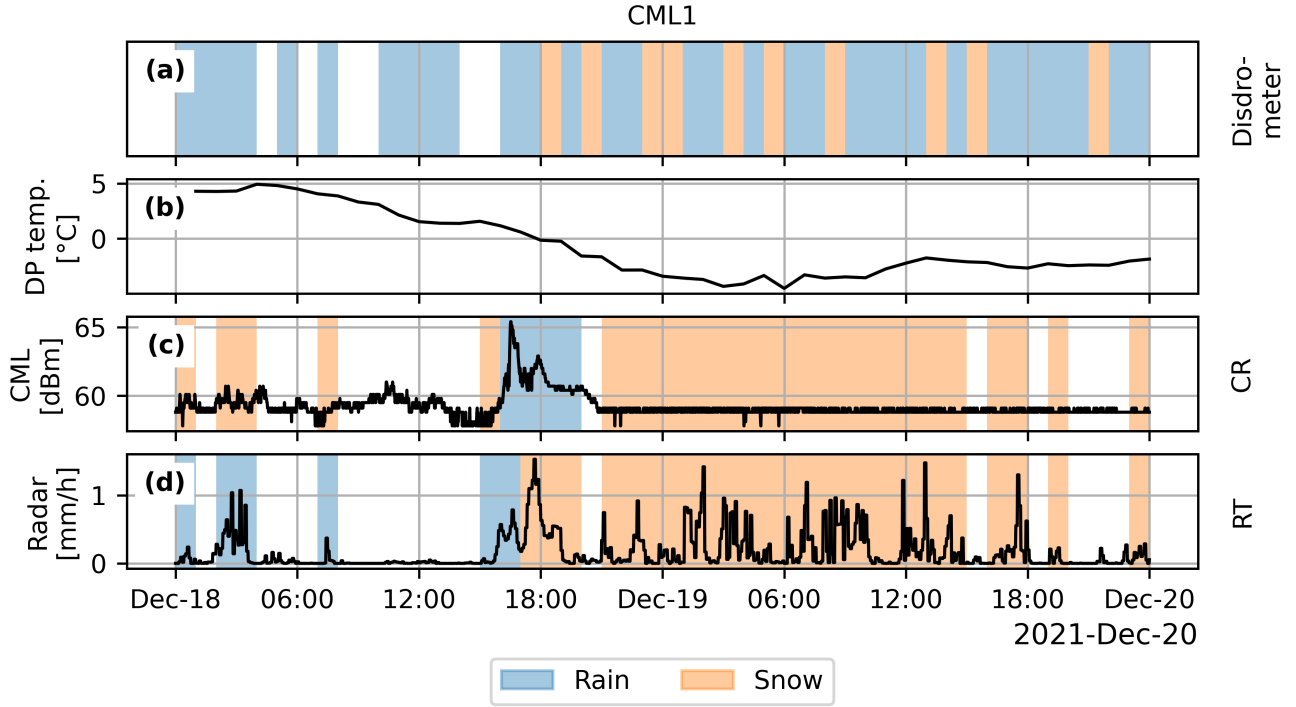
Figure 3. Time series for CML1 located in the eastern mountain area of Fig. 2. Dew point temperature (**b**), CML signal loss (**c**), and radar rainfall (**d**). Shaded areas indicate the precipitation type (rain or snow) estimated by the disdrometer (**a**), the CR method (**c**), and the RT method (**d**).

Examining the time series for CML1 and CML2 (Fig. 3 and Fig. 4), we observe that before 18:00 on December 18th, the dew point temperature (**b**) is mostly above 0 degrees, and the CML signal level fluctuates markedly (**c**), especially during periods when the weather radar estimates rainfall. After 18:00, as the temperature drops well below 0 degrees, the CML signal loss shows a different pattern with much less fluctuation. Around 18:00, the CR method, RT method, and disdrometer all estimate rainfall. After 18:00, the CR and RT methods estimate snow, while the disdrometer shifts between rain and snow. Before 18:00, the RT method estimates some rainfall while the CR method estimates snow, possibly because the rainfall event was not strong enough for the CML wet detection algorithm to identify it as rainfall.

The time series for CML3 indicates a different climatological pattern compared to CML1 and CML2, with temperatures above zero before 18:00 on December 18th and hovering around zero degrees afterward (Fig. 5). Observing the CML time series, we see that the signal loss fluctuates during all time steps when the radar estimates precipitation. The disdrometer primarily indicates rainfall, except for a period from 00:00 to 09:00 on December 19th, when it shows a mixture of rain and snow. In contrast, the RT method indicates a longer snowy period, lasting from 19:00 on the 18th to 14:00 on the 19th. The CR method primarily estimates rainfall but identifies short snowy periods around the disdrometers snow period, and estimates rainfall when the disdrometer indicates snow.
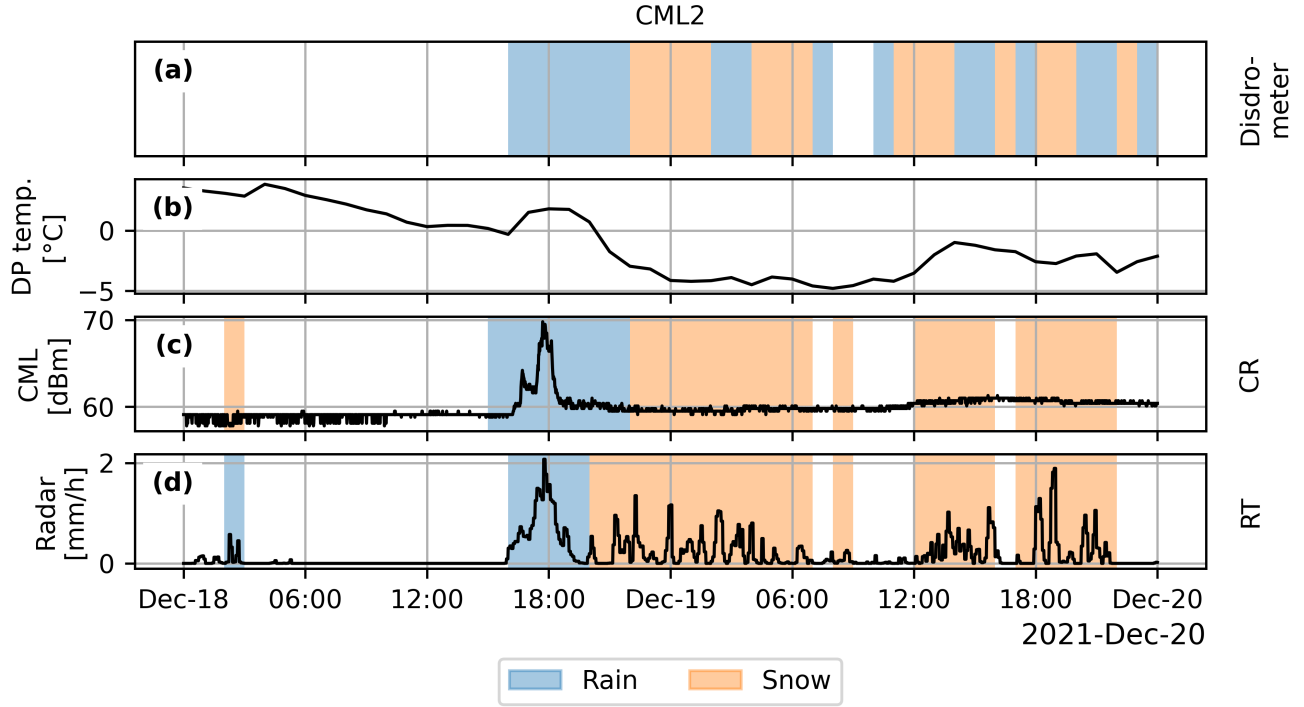
Figure 4. Time series for CML2 located in the southern mountain area of Fig. 2. Dew point temperature **(b)**, CML signal loss **(c)**, and radar rainfall **(d)**. Shaded areas in indicate the precipitation type (rain or snow) estimated by the disdrometer **(a)**, the CR method **(c)**, and the RT method **(d)**.

3.2 Overview of the data as a function of dew point temperature

245 To get an overview of the full dataset used in the study, we counted the total number of rainy and snowy hours estimated by the disdrometers, RT method, and CR method for 1-degree dew point temperature intervals between -20 and 20 degrees (Fig. 6). Our data covers the full temperature range, with most observations concentrated between -10 and 10 degrees. The disdrometers record snow mainly below zero degrees **(a)**, with some snow events slightly above zero. Most rainy hours recorded by the disdrometers occur above zero degrees, but there are also a substantial number of rainy hours recorded below zero. The

250 CR method also estimates rainy hours below zero degrees, though less frequently than the disdrometers, and it estimates a significant number of snowy hours above zero degrees **(c)**. The RT method, by definition, predicts rainy hours above zero degrees and snowy hours below zero degrees **(b)**. Additionally, we observe that the RT method estimates fewer rainy hours than the CR method, even above zero degrees.

The difference between the estimated CML rainfall amounts and the radar rainfall amounts is plotted as a function of dew

255 point temperature (Fig. 7 **(a)**). For dew point temperatures below -2 degrees, there is a positive bias where the radar generally estimates more precipitation. Between 0 and 2.5 degrees, there is a stronger negative bias where the CML estimates more
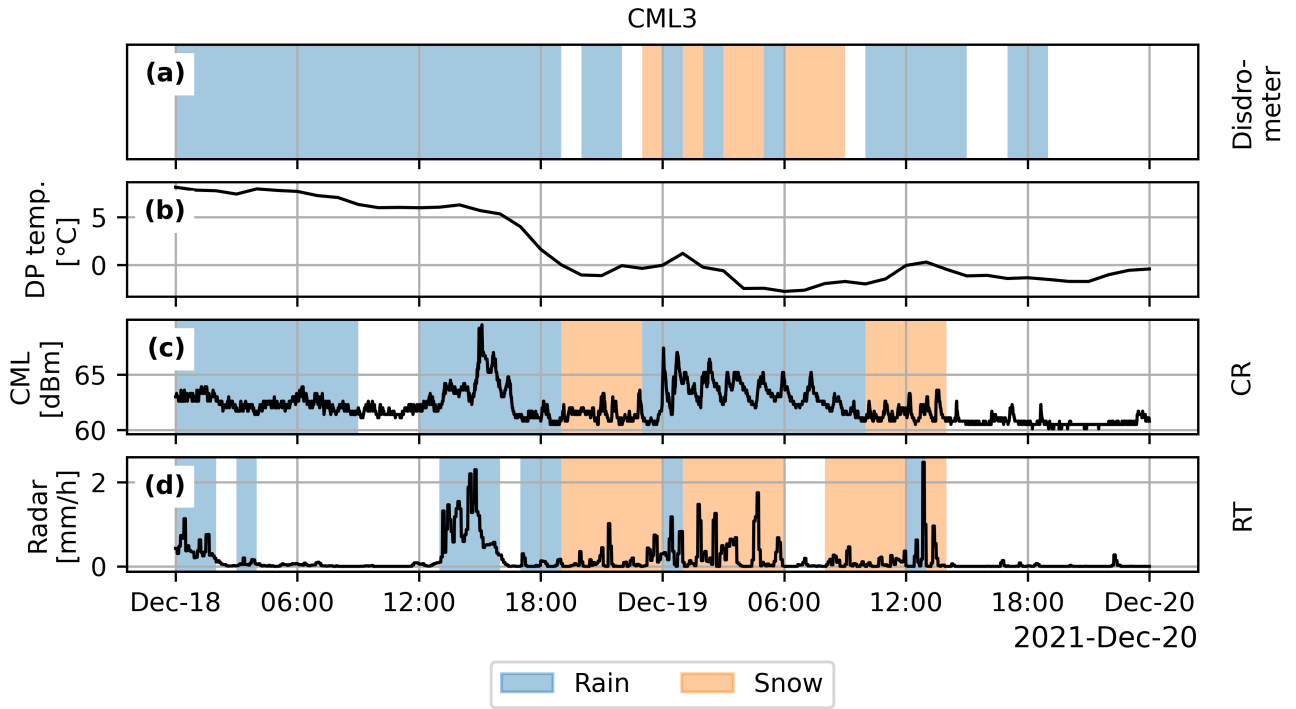
Figure 5. Time series for CML3 located in the north western coastal area of Fig. 2. Dew point temperature (**b**), CML signal loss (**c**), and radar rainfall (**d**). Shaded areas in indicate the precipitation type (rain or snow) estimated by the disdrometer (**a**), the CR method (**c**), and the RT method (**d**).
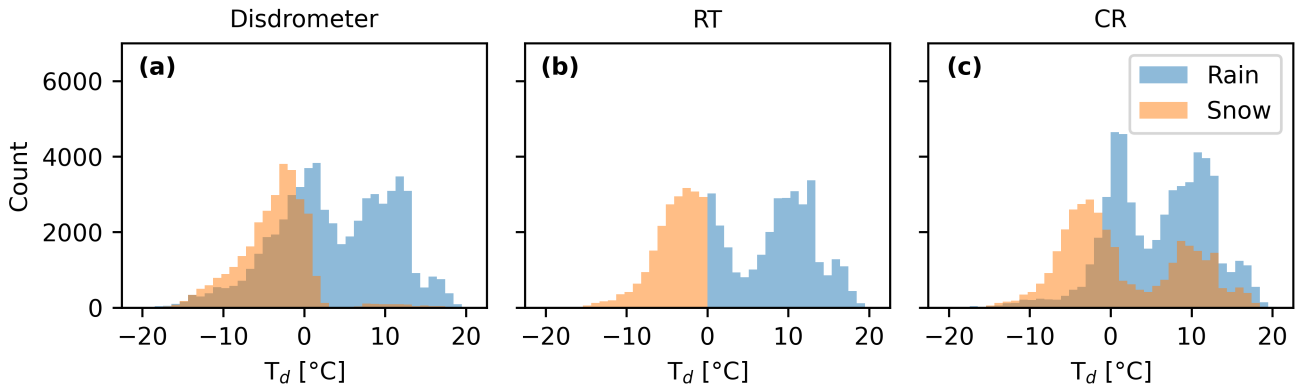
Figure 6. Number of hours classified as snowy or rainy for dew point temperature (T_d) intervals of 1 degree ranging between -20 to 20 degrees for the disdrometers (**a**), RT (**b**) and CR (**c**) estimates.

precipitation. For dew point temperatures above 4 degrees, the CML and radar estimates show a similar spread. In panels **(b)** and **(c)** the color of the cell indicate the proportion of rainy or snowy hours over total hours for each cell in panel **(a)**. Generally, there is more rainfall in observations above -2.5 degrees and more snow in observations below 2.5 degrees. Additionally, for events where the CML estimates more rainfall (negative bias), there are more rainy hours as observed by the disdrometer.

3.3 The performance of the CR method vs. the RT method

The performance of each CML-disdrometer pair for the RT and CR methods is compared on the summer and winter dataset using scatter density plots (Fig. 8, **(a, b, c, d, e)**). In the lower row **(f, g, h, i, j)**, the mean dew point temperature of each CML disdrometer pair is shown. Note that some cells consist of several CML-disdrometer pairs and that the indicated temperature then is the average of all pairs in the cell. In terms of accuracy **(a, f)**, both the CR and RT methods perform similarly well, with a few CMLs performing less well using the CR method. For precision **(b, g)**, we observe that, on average, the RT method outperforms the CR method, indicating that the RT methods positive predictions are more trustworthy than those of the CR method. However, the CMLs where the CR method performs less well tend to have an average temperature above 5 degrees, while for colder temperatures, the RT and CR precision scores are more similar. In terms of recall **(c, h)**, the CR method performs slightly better than the RT method, indicating that the CR method is better at correctly identifying the disdrometer precipitation type. Looking at the F1 score **(d, i)**, which combines the precision and recall score, we observe that the CR method performs worse on average when the temperature is above 5 degrees, but better when the temperature is below 5 degrees. Lastly, looking at the MCC score **(e, j)**, the CR method outperforms the RT method for most CML-disdrometer pairs.

To investigate the effect of temperature on the CR and RT predictions we plotted the multi-label confusion matrix of the two methods for the three temperature intervals -20 °C to -2 °C **(a, d)**, -2 °C to 2 °C **(b, e)** and 2 °C to 20 °C **(c, f)** (Fig. 9). The corresponding accuracy, precision, recall, F1 and MCC scores for the individual classes (rain and snow) as well as the multiclass score are shown in Table 3. We can observe that, compared to the RT method, the CR method generally identifies more correct rainfall events. It also identifies more snowfall events in the temperature interval -2 to 2 degrees.

4 Discussion

4.1 Evaluation of the disdrometers performance

The disdrometer data suggest that rain is more frequent below zero degrees than snow is above zero degrees (Fig. 6), which could indicate that the disdrometer overestimates the number of rainy hours. For example, looking at the CML time series (Fig. 3), the disdrometer shows a mix of rain and snow, while the CR and RT methods indicate only snow. This discrepancy could be due to the spatial distance between disdrometers and CMLs, with temperature differences at these locations possibly causing rain to be recorded at colder temperatures. However, if this effect were significant, we would also expect to see more snow recorded at temperatures above zero degrees, which we do not observe. Another explanation for these discrepancies could be the aggregation method, where rainy hours are given priority over snowy hours, creating the impression that there are
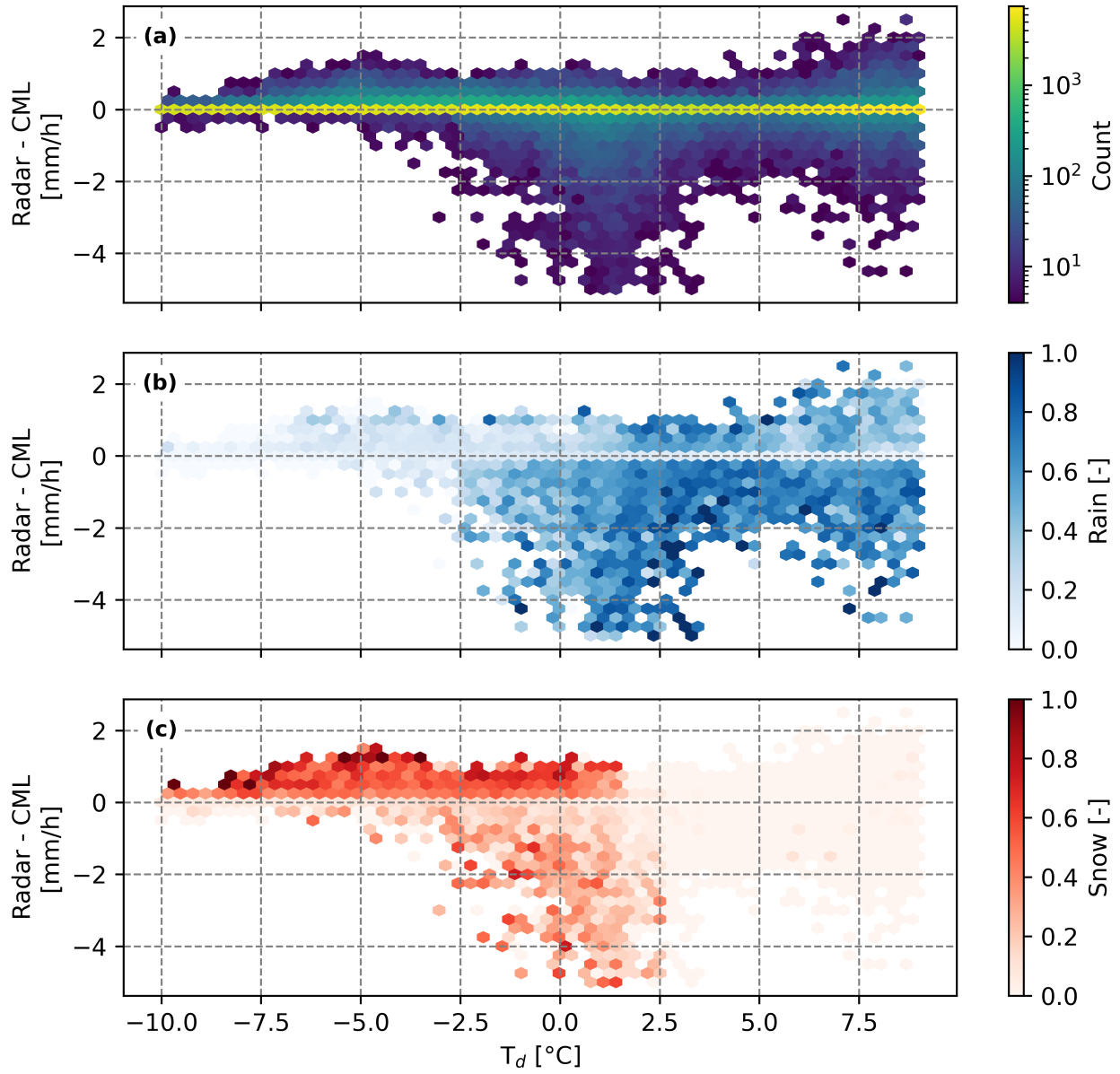
Figure 7. (a): Difference between hourly precipitation amounts measured by the radar and CML for dew point temperature (T_d) intervals of 1 degree ranging between -10 to 10 degrees. **(b, c):** Ratio of rain and snow in each cell as observed by the disdrometer. Cells with less than 4 events are not shown.
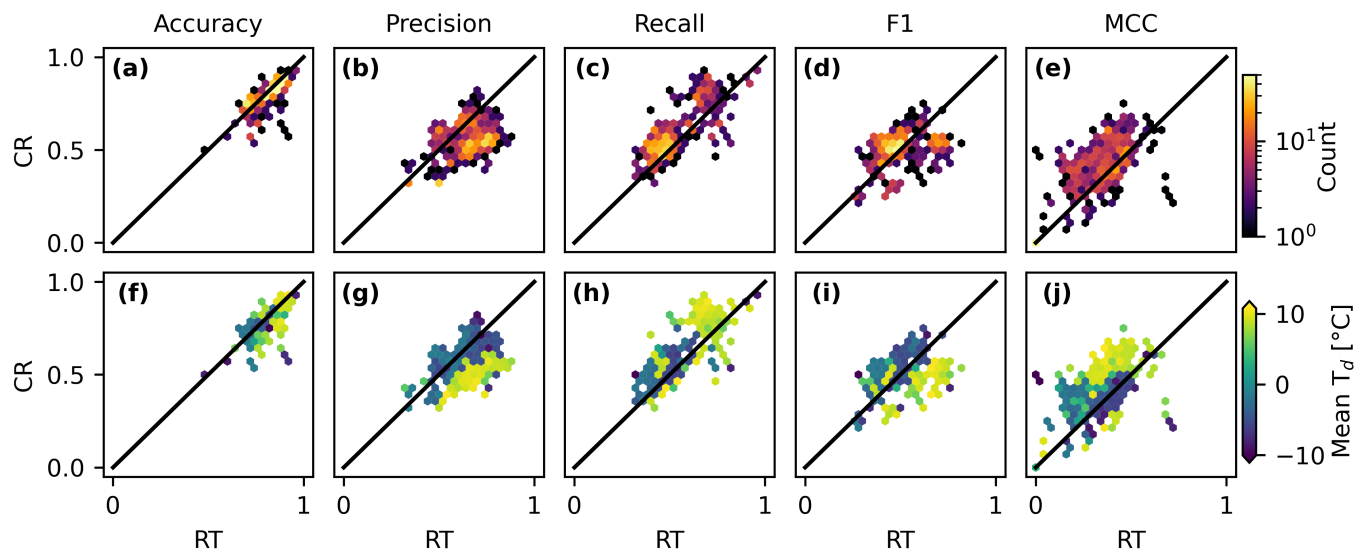
Figure 8. Scatter density plots **(a, b, c, d, e)** comparing the accuracy, precision, recall, F1 and MCC score for the CR and RT method for each CML-disdrometer pairs. Average dew point temperature of each cell **(f, g, h, i, j)**.
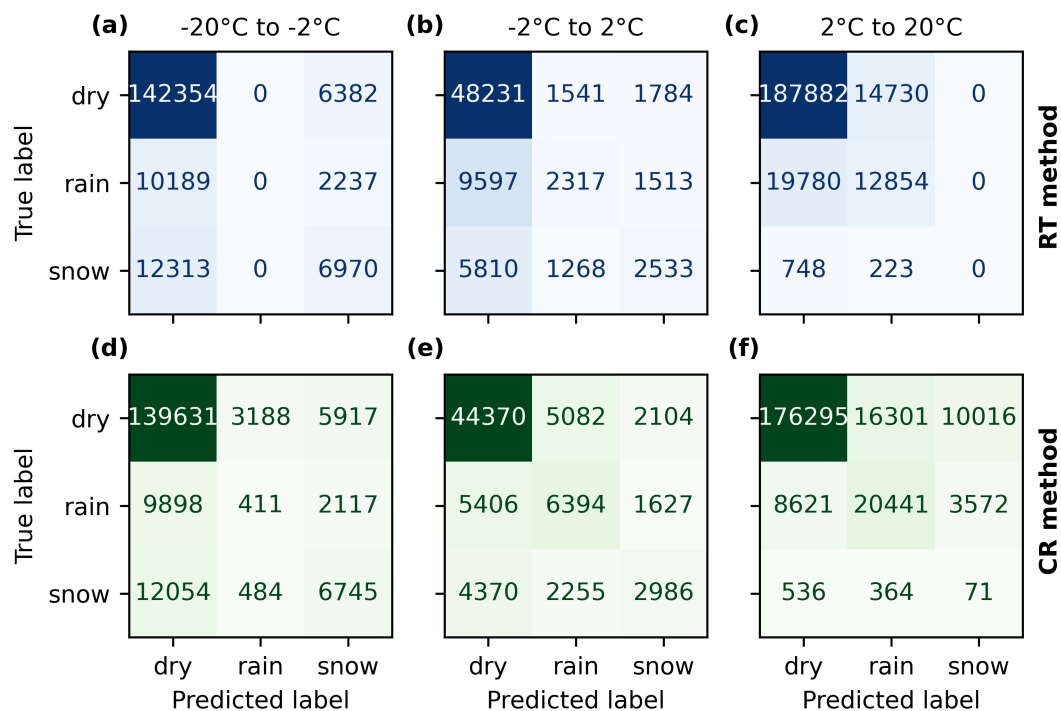
Figure 9. Confusion matrices for the RT **(a, b, c)** and CR **(d, e, f)** method for three temperature intervals.

Table 3. Accuracy, precision, recall, F1 and MCC score for the RT and CR method for different temperature intervals. The "Rain", "Snow" and "Multi" columns indicates wether the metric was evaluated against rainfall only, snow only or if it used the generalized multiclass metric to evaluate both rain and snow.

	-20°C to -2°C			-2°C to 2°C			2°C to 20°C			All temperatures		
	Rain	Snow	Multi	Rain	Snow	Multi	Rain	Snow	Multi	Rain	Snow	Multi
Accuracy RT	0.93	0.88	0.83	0.81	0.86	0.71	0.85	1.00	0.85	0.88	0.93	0.82
Accuracy CR	0.91	0.89	0.81	0.81	0.86	0.72	0.88	0.94	0.83	0.88	0.91	0.81
Precision RT	0.93	0.69	0.66	0.65	0.67	0.55	0.68	1.00	0.68	0.68	0.70	0.59
Precision CR	0.52	0.69	0.47	0.68	0.67	0.58	0.74	0.50	0.50	0.71	0.62	0.56
Recall RT	0.50	0.65	0.44	0.56	0.61	0.46	0.66	0.50	0.44	0.61	0.65	0.51
Recall CR	0.51	0.65	0.44	0.68	0.63	0.55	0.77	0.51	0.52	0.70	0.64	0.56
F1 RT	0.48	0.67	0.44	0.57	0.63	0.47	0.67	0.50	0.45	0.63	0.67	0.53
F1 CR	0.50	0.67	0.45	0.68	0.64	0.56	0.76	0.49	0.50	0.71	0.63	0.56
MCC RT	0.00	0.34	0.30	0.19	0.27	0.28	0.34	0.00	0.34	0.28	0.34	0.32
MCC CR	0.02	0.34	0.27	0.35	0.30	0.39	0.52	0.00	0.47	0.41	0.25	0.39

more rainy hours below zero degrees. However, if the disdrometer was correct and 10 minutes of an hour were indeed rainy, that would still represent a significant amount of rain during that hour. Moreover, comparing the CR rain distribution with the disdrometer rain distribution (Fig. 6), we can see that the CR method observes fewer rainy hours below zero degrees, indicating that the disdrometers overestimate the number of rainy hours below zero degrees.

One explanation for this overestimation could be that wet snow makes the disdrometer alternate between snow and rain, creating the impression that there is more rain below zero degrees. Moreover, different precipitation type sensors are also known to disagree during mixed precipitation events (Bloemink, 2005; Pickering et al., 2021), indicating that these events are hard to classify. However, while wet snow could explain some of the rainfall events below zero degrees, the large proportion of rainy hours below -10 degrees remains puzzling, as wet snow is not expected at such low temperatures. Another explanation could be misclassification by the disdrometer due to factors such as strong winds, particles falling through the edges of the sampling area and splashing. Although correction algorithms exist (Friedrich et al., 2013), they typically require the full velocity-drop size distribution matrix, which our disdrometers do not provide. This limitation may lead to less accurate classifications. Additionally, cars spraying water from salted roads could contribute to the high number of rainfall events recorded below zero degrees. Consequently, while the disdrometers provides valuable estimates, they do not perfectly represent the ground truth, especially during mixed precipitation events.

4.2 The case study

The case study indicated that the CR and RT methods estimated a similar number of snow events in the mountains, while along the coast (for instance at CML3), the CR estimates were more in line with the disdrometer estimates, suggesting an advantage

of using the CR method in certain climatic zones. This could be due to the warmer conditions along the coast, which keep the temperature around zero degrees, a range where the RT method has more uncertainties. However, looking at the time series of CML3 (Fig. 5) we see that the CR method estimates rainfall during the true snow event, lasting from 00:00 to 10:00 on the 19th of December. It also wrongly estimates snowfall before and after the true snowfall event. Thus, while the case study map

310   suggests a better agreement between the CR and disdrometer estimates (Fig. 2), there is still a significant discrepancy between the CR and disdrometer estimates in the hourly time series (Fig. 5). This discrepancy could be due to the spatial difference between the CML and disdrometer or disdrometer misclassification, as discussed above. Another explanation could be that the disdrometers classify mixed precipitation, such as wet snow, as snow, while the CMLs classify wet snow as rainfall, leading to a misclassification by the CMLs. This phenomenon is clearly observable during the true snowfall event lasting from 00:00 to

315   10:00 on the 19th of December (Fig. 5), where the CML estimates a long rainy period and the disdrometer estimates a mixture of rainfall and snow.

4.3   The CR and RT methods classification performance

For snowfall classification at temperatures between -2 and 2 degrees, the CR method holds a slight advantage over the RT method, as reflected in a slightly higher MCC (0.3 vs 0.27) and recall score (0.63 vs 0.61) (Table 3). This indicates that the CR

320   method is slightly better at identifying true snow events (higher recall) while maintaining reliable estimates (equal precision of 0.67). Looking at the confusion matrix for the same temperature interval, we observe that compared to the RT method, the CR method correctly identified 2986 true snowy hours, an increase of 453 hours, while wrongly classifying 3731 hours as snow, an increase of 434 hours (Fig. 9). In other words, the CR method identifies more true snowfall events while also wrongly classifying rainy and dry events as snow. The large number of false snow events, also observable at temperatures above 2

325   degrees, estimated by CR method might be due to the CML rainfall detection algorithm not being triggered by small rainfall events. At temperatures below -2 degrees (Fig. 6, both the CR and RT method snow classification produced recall scores of 0.65, indicating that the weather radar misses many of the snowfall events recorded by the disdrometers. This could be due to the spatial difference between the CML and disdrometer or disdrometer misclassification, as discussed above. Another explanation could be that blowing winds or road traffic transport snow horizontally, causing the disdrometers to detect snow

330   that does not originate from the sky.

In terms of rainfall classification, the CR method performs as well as or outperforms the RT method for all temperatures above -2 degrees (Table 3). For instance, for temperatures above 2 degrees, the binary accuracy score for rainfall increases from 0.85 with the RT method to 0.88 with the CR method, and the binary MCC for rainfall increases from 0.34 to 0.52. However, both the RT and CR methods still miss many of the rainfall events observed by the disdrometer, which is evident in their recall

335   scores of 0.66 and 0.77, respectively. As discussed above, this could be due to the spatial difference between the CML and disdrometer, or for instance splashing from the roads, leading the disdrometers to estimate rainfall that is not detected by the CML or weather radar. The increased performance of the CR method, compared to the RT method, could be due to radar overshooting or the radar beam being blocked by mountains.

4.4 Uncertainties, the impact of the aggregation method and mixed precipitation types

340 The impact of mixed precipitation, such as wet snow, on the observation methods (disdrometers, CR method, and RT method) remains a significant source of uncertainty in this study. This uncertainty arises from the fact that none of the observation methods can reliably classify mixed precipitation. Additionally, accurately classifying hours that may contain both snow and rain when aggregating the data to hourly intervals poses a challenge. One solution is to introduce a mixed class, classifying hours with both snow and rain as mixed precipitation. However, it remains unclear whether true mixed precipitation, like wet

345 snow, would consistently cause the disdrometer, CR, and RT methods to alternate between detecting rain and snow, which could make the mixed class less physically meaningful and lead to inconsistent representations across different estimation methods. While other studies, such as Pickering et al. (2021), aggregated multiple precipitation type data from different sensors to longer periods using a boolean algorithm, we found that the sensors used in our study differed too much for a similar approach. For instance, the RT method uses temperature data with hourly resolution, which complicates accurately capturing hours with

350 both wet and solid precipitation types. While some studies introduce mixed precipitation estimates by classifying precipitation within a fixed temperature interval as mixed (Harpold et al., 2017), the true precipitation type within this interval could still be purely rain or purely snow, leading to inaccurate classifications. Furthermore, since the radar might estimate precipitation slightly before the CML, the CR method is prone to estimate snow before rainfall events, leading to an overestimation of mixed precipitation. This could be addressed by aggregating the CML wet period so that the radar precipitation estimates fall

355 inside the wet period, but this would require further tuning to avoid estimating too many rainfall events at the expense of fewer true mixed events. This work uses a simplified aggregation method in order to avoid introducing too many parameters. We found that, while this approach produces a higher rain to snow ratio for negative temperatures, the assumptions are stated more explicit, and the final results and conclusion remain similar to what we got using other aggregation methods.

Around zero degrees, the CMLs estimate larger rainfall amounts compared to the weather radar (Fig. 7). The same tem-
360 perature interval is also characterized by the disdrometers observing both rainfall and snow. This suggests that significant discrepancies between the CML and radar estimates around zero degrees may be attributed to wet snow. This effect has been observed before in previous studies, such as Overeem et al. (2016) and Graf et al. (2020), where a marked positive CML bias during the winter months was observed. Further, Fig. 7 reveal that the CML bias as a function of temperature, follows a smooth transition. This indicate that wet snow, as observed by the CML, do not belong to a homogeneous group, but instead follow a
365 gradual transition from snow to rainfall while melting.

While studies such as Gjertsen and Ødegaard (2005), Casellas et al. (2021), and Saltikoff et al. (2015) have evaluated the performance of temperature-based precipitation phase classification methods, these studies typically vary in methodology, ter-rain complexity, radar technology, and the instruments used to estimate the ground truth. This variability introduces challenges when comparing results across different studies. Although the disdrometers used in this study provide a large dataset, they have
370 some limitations; in particular, the large number of rainy events recorded below zero degrees and the lack of mixed class clas-sification introduce uncertainties specific to this study. Further, any type of wet precipitation can cause the CML signal level to drop, potentially leading to precipitation being falsely classified as rainfall. Another source of uncertainty is the spatial distance

between the disdrometer and the CML, where for instance temperature variations due to elevation and spatial differences can affect precipitation classification. Moreover, the temperature model used is based on model data, and could be improved by using ground based sensors. Combined, these factors introduce large uncertainties in this study, and further make it challenging to directly compare the CR and RT estimates in this study to those from similar studies.

Nevertheless, our study demonstrates that CMLs can be used to enhance classification of snow and rainfall around zero degrees, which are useful for hydrological applications such as in predicting hydropower production, flooding, avalanches and slush avalanches.

5 Conclusions

In this work, we have compared two methods for classifying rain and snow. The "radar-temperature" (RT) method works by classifying weather radar precipitation below zero degrees as snow and above as rain, using dew-point temperature derived from downscaled ERA5 data. The "CML-radar" (CR) method, exploits the fact that dry snow causes minimal signal attenuation in the CML signal level, and works by classifying time steps where the weather radar detects precipitation, and the CMLs do not detect precipitation, as snowy. Time steps where the CML detects rainfall are set to rainy. The estimates were compared to estimates from nearby disdrometers located along roads in Norway.

Our results show that the CR method outperforms the RT method for dry snow detection between -2 and 2 degrees and, in general, for rainfall detection, suggesting that CMLs can be used to better classify rain and snow. Further, our results indicate that wet snow is classified as rainfall by the CMLs and that during these events the disdrometers tends to estimate a mix of rainfall and snow. Future work should investigate methods for CML wet snow detection, preferably using several different precipitation type sensors as ground truth, as suggested by Pickering et al. (2021). Future work should also investigate how the CR estimates impact hydrological models.

Overall, our findings suggest a new application for using CMLs to identify dry snow and contribute to better understanding on how CMLs behave during events of mixed precipitation.

Code and data availability. The software used for CML processing software is available under https://github.com/pycomlink/pycomlink/tree/master. Disdrometer data is available from (Frost, 2024). Radar data is available from (THREDDS, 2024). CML data were provided by Ericsson and are not publicly available.

Author contributions. Conceptualization: EØ, JA, RB. Data curation: EØ. Methodology: EØ, JA, RG, RB, MW, NOK, CC, VN. Software: EØ, CC. Supervision: VN, MW, NOK, RB. Writing – original draft preparation: EØ. Writing – review and editing: EØ, RG, JA, RB, MW, NOK, CC, VN.

Competing interests. The contact author has declared that neither of the authors has any competing interests.

Acknowledgements. The authors thank co-supervisor Etienne Leblois for nice discussions. We would also like to thank Ericsson for providing CML data. This work is funded by the Norwegian University of Life Sciences and the German Research Foundation via the SpraiLINK project (Grant CH-1785/2-1).

References

Berne, A. and Krajewski, W.: Radar for hydrology: Unfulfilled promise or unrecognized potential?, Advances in Water Resources, 51, 357–366, https://doi.org/10.1016/j.advwatres.2012.05.005, 2013.

Blettner, N., Fencl, M., Bareš, V., Kunstmann, H., and Chwala, C.: Transboundary Rainfall Estimation Using Commercial Microwave Links, Earth and Space Science, 10, https://doi.org/10.1029/2023EA002869, 2023.

Bloemink, H.: Precipitation type from the Thies disdrometer, in: WMO Tech. Conf. on Meteorological and Environmental Instruments and Methods of Observation (TECO-2005), pp. 1–7, World Meteorological Organization, Bucharest, Romania, https://library.wmo.int/viewer/41919/download?file=wmo-td_1265.pdf&type=pdf&navigator=1, accessed: 2025-01-23, 2005.

Casellas, E., Bech, J., Veciana, R., Pineda, N., Miró, J. R., Moré, J., Rigo, T., and Sairouni, A.: Nowcasting the precipitation phase combining weather radar data, surface observations, and NWP model forecasts, Quarterly Journal of the Royal Meteorological Society, 147, 3135–3153, https://doi.org/10.1002/qj.4121, 2021.

Chandrasekar, V., Keränen, R., Lim, S., and Moisseev, D.: Recent advances in classification of observations from dual polarization weather radars, Atmospheric Research, 119, 97–111, https://doi.org/10.1016/j.atmosres.2011.08.014, 2013.

Cherkassky, D., Ostrometzky, J., and Messer, H.: Precipitation Classification Using Measurements From Commercial Microwave Links, IEEE Transactions on Geoscience and Remote Sensing, 52, 2350–2356, https://doi.org/10.1109/TGRS.2013.2259832, 2014.

Chicco, D. and Jurman, G.: The advantages of the Matthews correlation coefficient (MCC) over F1 score and accuracy in binary classification evaluation, BMC Genomics, 21, 6, https://doi.org/10.1186/s12864-019-6413-7, 2020.

Chwala, C., Polz, J., Graf, M., Sereb, D., Blettner, N., Keis, F., and Boose, Y.: pycomlink/pycomlink: v0.3.2, https://doi.org/https://doi.org/10.5281/ zenodo.4810169, 2023.

Elmore, K. L.: The NSSL Hydrometeor Classification Algorithm in Winter Surface Precipitation: Evaluation and Future Development, Weather and Forecasting, 26, 756–765, https://doi.org/10.1175/WAF-D-10-05011.1, 2011.

Feiccabrino, J. M.: Precipitation phase uncertainty in cold region conceptual models resulting from meteorological forcing time-step intervals, Hydrology Research, 51, 180–187, https://doi.org/10.2166/nh.2020.080, 2020.

Friedrich, K., Kalina, E. A., Masters, F. J., and Lopez, C. R.: Drop-Size Distributions in Thunderstorms Measured by Optical Disdrometers during VORTEX2, Monthly Weather Review, 141, 1182–1203, https://doi.org/10.1175/MWR-D-12-00116.1, 2013.

Frost: https://frost.met.no/index.html, 2024.

Førland, E., Allerup, P., Dahlström, B., Elomaa, E., Jónsson, T., Madsen, H., Perälä, J., Rissanen, P., Vedin, H., and Vejen, F.: Manual for Operational Correction of Nordic Precipitation Data, DNMI-report, Norske meteorologiske institutt, https://books.google.no/books?id=HLIKcgAACAAJ, 1996.

Gjertsen, U. and Ødegaard, V.: The water phase of precipitation—a comparison between observed, estimated and predicted values, Atmospheric Research, 77, 218–231, https://doi.org/10.1016/j.atmosres.2004.10.030, 2005.

Gorodkin, J.: Comparing two K-category assignments by a K-category correlation coefficient, Computational Biology and Chemistry, 28, 367–374, https://doi.org/10.1016/j.compbiolchem.2004.09.006, 2004.

Graf, M., Chwala, C., Polz, J., and Kunstmann, H.: Rainfall estimation from a German-wide commercial microwave link network: optimized processing and validation for 1 year of data, Hydrology and Earth System Sciences, 24, 2931–2950, https://doi.org/10.5194/hess-24-2931-2020, 2020.

Grazioli, J., Tuia, D., and Berne, A.: Hydrometeor classification from polarimetric radar measurements: a clustering approach, Atmospheric Measurement Techniques, 8, 149–170, https://doi.org/10.5194/amt-8-149-2015, 2015.

Hansryd, J., Li, Y., Chen, J., and Ligander, P.: Long term path attenuation measurement of the 71–76 GHz band in a 70/80 GHz microwave link, in: Proceedings of the Fourth European Conference on Antennas and Propagation, pp. 1–4, 2010.

445 Harder, P. and Pomeroy, J.: Estimating precipitation phase using a psychrometric energy balance method, Hydrological Processes, 27, 1901–1914, https://doi.org/10.1002/hyp.9799, 2013.

Harder, P. and Pomeroy, J. W.: Hydrological model uncertainty due to precipitation-phase partitioning methods, Hydrological Processes, 28, 4311–4327, https://doi.org/10.1002/hyp.10214, 2014.

Harpold, A. A., Kaplan, M. L., Klos, P. Z., Link, T., McNamara, J. P., Rajagopal, S., Schumer, R., and Steele, C. M.: Rain or snow: hydrologic
450 processes, observations, prediction, and research needs, Hydrology and Earth System Sciences, 21, 1–22, https://doi.org/10.5194/hess-21-1-2017, 2017.

Hestnes, E.: A Contribution to the Prediction of Slush Avalanches, Annals of Glaciology, 6, 1–4, https://doi.org/10.3189/1985AoG6-1-1-4, 1985.

ITU, R.: RECOMMENDATION ITU-R P.838-3 Specific attenuation model for rain for use in prediction methods, pp. 1–8, 2005.

455 Jennings, K. S., Winchell, T. S., Livneh, B., and Molotch, N. P.: Spatial variation of the rain–snow temperature threshold across the Northern Hemisphere, Nature Communications, 9, 1148, https://doi.org/10.1038/s41467-018-03629-7, 2018.

Jurman, G., Riccadonna, S., and Furlanello, C.: A Comparison of MCC and CEN Error Measures in Multi-Class Prediction, PLoS ONE, 7, e41 882, https://doi.org/10.1371/journal.pone.0041882, 2012.

Kienzle, S. W.: A new temperature based method to separate rain and snow, Hydrological Processes, 22, 5067–5085,
460 https://doi.org/10.1002/hyp.7131, 2008.

Kochendorfer, J., Earle, M., Rasmussen, R., Smith, C., Yang, D., Morin, S., Mekis, E., Buisan, S., Roulet, Y.-A., Landolt, S., Wolff, M., Hoover, J., Thériault, J. M., Lee, G., Baker, B., Nitu, R., Lanza, L., Colli, M., and Meyers, T.: How Well Are We Measuring Snow Post-SPICE?, Bulletin of the American Meteorological Society, 103, E370–E388, https://doi.org/10.1175/BAMS-D-20-0228.1, 2022.

Kuhn, M.: Micro-Meteorological Conditions for Snow Melt, Journal of Glaciology, 33, 24–26, https://doi.org/10.3189/S002214300000530X,
465 1987.

Lamb, D. and Verlinde, J.: Physics and Chemistry of Clouds, Cambridge University Press, ISBN 9780521899109, https://doi.org/10.1017/CBO9780511976377, 2011.

Lawrence, M. G.: The Relationship between Relative Humidity and the Dewpoint Temperature in Moist Air: A Simple Conversion and Applications, Bulletin of the American Meteorological Society, 86, 225–234, https://doi.org/10.1175/BAMS-86-2-225, 2005.

470 Leijnse, H., Uijlenhoet, R., and Stricker, J. N. M.: Rainfall measurement using radio links from cellular communication networks, Water Resources Research, 43, 1–6, https://doi.org/10.1029/2006WR005631, 2007.

Leijnse, H., Uijlenhoet, R., and Stricker, J.: Microwave link rainfall estimation: Effects of link length and frequency, temporal sampling, power resolution, and wet antenna attenuation, Advances in Water Resources, 31, 1481–1493, https://doi.org/10.1016/j.advwatres.2008.03.004, 2008.

475 Leroux, N. R., Vionnet, V., and Thériault, J. M.: Performance of precipitation phase partitioning methods and their impact on snowpack evolution in a humid continental climate, Hydrological Processes, 37, https://doi.org/10.1002/hyp.15028, 2023.

Loth, B., Graf, H., and Oberhuber, J. M.: Snow cover model for global climate simulations, Journal of Geophysical Research: Atmospheres, 98, 10 451–10 464, https://doi.org/10.1029/93JD00324, 1993.

Lussana, C., Seierstad, I. A., Nipen, T. N., and Cantarello, L.: Spatial interpolation of two-metre temperature over Norway based on the combination of numerical weather prediction ensembles and in situ observations, Quarterly Journal of the Royal Meteorological Society, 145, 3626–3643, https://doi.org/10.1002/qj.3646, 2019.

Lussana, C., Nipen, T. N., Seierstad, I. A., and Elo, C. A.: Ensemble-based statistical interpolation with Gaussian anamorphosis for the spatial analysis of precipitation, Nonlinear Processes in Geophysics, 28, 61–91, https://doi.org/10.5194/npg-28-61-2021, 2021.

Löffler-Mang, M. and Joss, J.: An Optical Disdrometer for Measuring Size and Velocity of Hydrometeors, Journal of Atmospheric and Oceanic Technology, 17, 130–139, https://doi.org/10.1175/1520-0426(2000)017<0130:AODFMS>2.0.CO;2, 2000.

Marks, D., Winstral, A., Reba, M., Pomeroy, J., and Kumar, M.: An evaluation of methods for determining during-storm precipitation phase and the rain/snow transition elevation at the surface in a mountain basin, Advances in Water Resources, 55, 98–110, https://doi.org/10.1016/j.advwatres.2012.11.012, 2013.

Marshall, J. S. and Palmer, W. M. K.: The distribution of raindrops with size, Journal of Meteorology, 5, 165–166, https://doi.org/10.1175/1520-0469(1948)005<0165:TDORWS>2.0.CO;2, 1948.

Matsuo, T., Sasyo, Y., and Sato, Y.: Relationship between Types of Precipitation on the Ground and Surface Meteorological Elements, Journal of the Meteorological Society of Japan. Ser. II, 59, 462–476, https://doi.org/10.2151/jmsj1965.59.4_462, 1981.

McCabe, G. J., Clark, M. P., and Hay, L. E.: Rain-on-Snow Events in the Western United States, Bulletin of the American Meteorological Society, 88, 319–328, https://doi.org/10.1175/BAMS-88-3-319, 2007.

Messer, H., Zinevich, A., and Pinhas, A.: Environmental Monitoring by Wireless Communication Networks, Science, 312, 17–18, https://www.jstor.org/stable/3846088, 2006.

MET: MET Nordic dataset, https://github.com/metno/NWPdocs/wiki/MET-Nordic-dataset, 2024.

Nešpor, V. and Sevruk, B.: Estimation of Wind-Induced Error of Rainfall Gauge Measurements Using a Numerical Simulation, Journal of Atmospheric and Oceanic Technology, 16, 450–464, https://doi.org/10.1175/1520-0426(1999)016<0450:EOWIEO>2.0.CO;2, 1999.

Ostrometzky, J., Cherkassky, D., and Messer, H.: Accumulated Mixed Precipitation Estimation Using Measurements from Multiple Microwave Links, Advances in Meteorology, 2015, 1–9, https://doi.org/10.1155/2015/707646, 2015.

Overeem, A., Leijnse, H., and Uijlenhoet, R.: Measuring urban rainfall using microwave links from commercial cellular communication networks, Water Resources Research, 47, https://doi.org/10.1029/2010WR010350, 2011.

Overeem, A., Leijnse, H., and Uijlenhoet, R.: Two and a half years of country-wide rainfall maps using radio links from commercial cellular telecommunication networks, Water Resources Research, 52, 8039–8065, https://doi.org/10.1002/2016WR019412, 2016.

Pastorek, J., Fencl, M., and Bareš, V.: Uncertainties in discharge predictions based on microwave link rainfall estimates in a small urban catchment, Journal of Hydrology, 617, 129 051, https://doi.org/10.1016/j.jhydrol.2022.129051, 2023.

Paulson, K. and Al-Mreri, A.: A rain height model to predict fading due to wet snow on terrestrial links, Radio Science, 46, https://doi.org/10.1029/2010RS004555, 2011.

Pedregosa, F., Varoquaux, G., Gramfort, A., Michel, V., Thirion, B., Grisel, O., Blondel, M., Prettenhofer, P., Weiss, R., Dubourg, V., Vanderplas, J., Passos, A., Cournapeau, D., Brucher, M., Perrot, M., and Duchesnay, E.: Scikit-learn: Machine Learning in Python, Journal of Machine Learning Research, 12, 2825–2830, 2011.

Pickering, B. S., Neely, R. R., Jeffery, J., Dufton, D., and Lukach, M.: Evaluation of Multiple Precipitation Sensor Designs for Precipitation Rate and Depth, Drop Size and Velocity Distribution, and Precipitation Type, Journal of Hydrometeorology, 22, 703–720, https://doi.org/10.1175/JHM-D-20-0094.1, 2021.

poligrain: Poligrain, https://github.com/OpenSenseAction/poligrain, 2024.

Polz, J., Chwala, C., Graf, M., and Kunstmann, H.: Rain event detection in commercial microwave link attenuation data using convolutional neural networks, Atmospheric Measurement Techniques, 13, 3835–3853, https://doi.org/10.5194/amt-13-3835-2020, 2020.

Pu, K., Liu, X., Hu, S., and Gao, T.: Hydrometeor Identification Using Multiple-Frequency Microwave Links: A Numerical Simulation, Remote Sensing, 12, 2158, https://doi.org/10.3390/rs12132158, 2020.

Saltikoff, E., Lopez, P., Taskinen, A., and Pulkkinen, S.: Comparison of quantitative snowfall estimates from weather radar, rain gauges and a numerical weather prediction model, Boreal Environment Research, 20, 2015.

Schleiss, M., Rieckermann, J., and Berne, A.: Quantification and Modeling of Wet-Antenna Attenuation for Commercial Microwave Links, IEEE Geoscience and Remote Sensing Letters, 10, 1195–1199, https://doi.org/10.1109/LGRS.2012.2236074, 2013.

Stewart, R. E.: Precipitation Types in the Transition Region of Winter Storms, Bulletin of the American Meteorological Society, 73, 287–296, https://doi.org/10.1175/1520-0477(1992)073<0287:PTITTR>2.0.CO;2, 1992.

Stewart, R. E., Thériault, J. M., and Henson, W.: On the Characteristics of and Processes Producing Winter Precipitation Types near 0°C, Bulletin of the American Meteorological Society, 96, 623–639, https://doi.org/10.1175/BAMS-D-14-00032.1, 2015.

THREDDS: https://thredds.met.no/thredds/catalog.html, 2024.

van Leth, T. C., Overeem, A., Leijnse, H., and Uijlenhoet, R.: A measurement campaign to assess sources of error in microwave link rainfall estimation, Atmospheric Measurement Techniques, 11, 4645–4669, https://doi.org/10.5194/amt-11-4645-2018, 2018.

Wolff, M. A., Isaksen, K., Petersen-Øverleir, A., Ødemark, K., Reitan, T., and Brækkan, R.: Derivation of a new continuous adjustment function for correcting wind-induced loss of solid precipitation: results of a Norwegian field study, Hydrology and Earth System Sciences, 19, 951–967, https://doi.org/10.5194/hess-19-951-2015, 2015.

Yuter, S. E., Kingsmill, D. E., Nance, L. B., and Löffler-Mang, M.: Observations of Precipitation Size and Fall Speed Characteristics within Coexisting Rain and Wet Snow, Journal of Applied Meteorology and Climatology, 45, 1450–1464, https://doi.org/10.1175/JAM2406.1, 2006.

Øydvin, E., Graf, M., Chwala, C., Wolff, M. A., Kitterød, N.-O., and Nilsen, V.: Technical Note: A simple feedforward artificial neural network for high temporal resolution classification of wet and dry periods using signal attenuation from commercial microwave links, EGUsphere [preprint], https://doi.org/https://doi.org/10.5194/egusphere-2024-647, 2024.